Mem. S.A.It. Vol. 90, 479

Memorie della

Empirical study of formamide formation around young O-type stars

V. Allen[1,2,3], A. López-Sepulcre[4,5], Á. Sánchez-Monge[6], V. M. Rivilla[7], and R. Cesaroni[7]

[1] NASA Goddard Space Flight Center, 8800 Greenbelt Road, Greenbelt, MD 20771, USA
e-mail: veronica.a.allen@nasa.gov
[2] Kapteyn Astronomical Institute, Landleven 12, 9747 AD Groningen, the Netherlands
[3] SRON, Landleven 12, 9747 AD Groningen, the Netherlands
[4] CNRS, IPAG, Univ. Grenoble Alpes, 414 Rue de la Piscine, 38000 Saint-Martin-d'Hères, France
[5] IRAM, 300 rue de la Piscine, 38406 Saint-Martin d'Hères, France
[6] I. Physikalisches Institut, Universität zu Köln, Zülpicher Strasse 77, 50937 Köln, Germany
[7] INAF-Osservatorio Astrofisico di Arcetri, Largo Enrico Fermi 5, I-50125 Florence, Italy

Abstract. Formamide (NH_2CHO) is an important prebiotic molecule as it has been proposed as a precursor to amino acids and other important molecules of life. In my talk, I detail the results of a high angular resolution (0.2″) ALMA observations of several different young high-mass stars and how the spatial extent and kinematics of formamide (NH_2CHO) in the surrounding gas compares to two of its possible parent species isocyanic acid (HNCO) and formaldehyde (H_2CO). This is important astrochemical work because there is debate about whether formamide is formed in ice and melts off once it becomes warm (from HNCO) or in already warm gas (from H_2CO). The results of this pilot study will be followed up with future ALMA observations.

Key words. stars: massive – ISM: individual objects: G17.64+0.16, G24.78+0.08, G345.49+1.47 – astrochemistry

1. Introduction

Formamide (NH_2CHO) is an important molecular species to study as it is thought to be a precursor to the simplest amino acid, glycine (NH_2CH_2COOH) (Saladino et al. 2012). The peptide bond (N-C=O) makes NH_2CHO especially relevant to astrobiology as pre-biotic molecules were likely delivered to an early Earth to help bring about the origin of life. As for formamide itself, there is disagreement about how it forms. Here we investigate two formation routes: (1) hydrogenation of isocyanic acid (HNCO) on dust grain ice mantles in the reactions HNCO + H $\rightarrow$ H_2NCO then H_2NCO + H $\rightarrow$ NH_2CHO (Charnley, S. B. 1997) which later sublimates into the gas or (2) reactions between H_2CO and NH_2 (which is especially abundant in photon-dominated regions) in warm gas (H_2CO + NH_2 $\rightarrow$ NH_2CHO+ H) (Kahane et al. 2013) (see Figure 1 for a visual illustration).

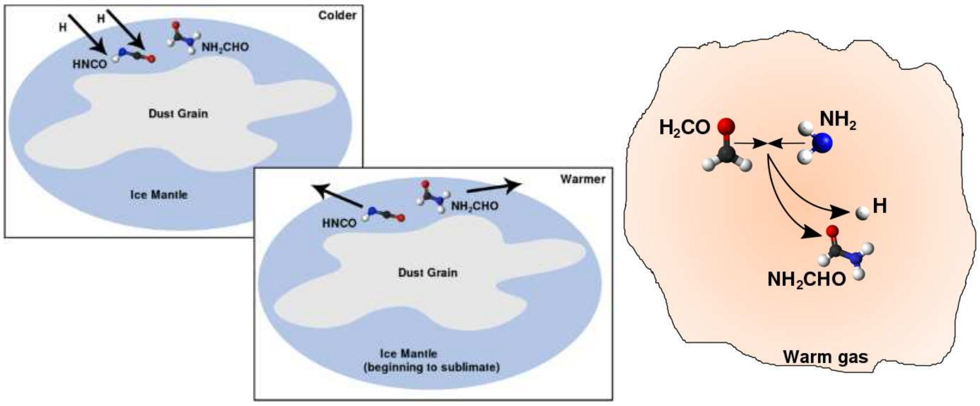

Fig. 1. Illustrations of the formation reactions for NH_2CHO. Hydrogenation of HNCO (left) and H_2CO + NH_2 (right).

Evidence has been presented supporting both formation pathways. Recent laboratory work by Kaňuchová et al. (2017) shows that NH_2CHO can be formed in cosmic-ray-irradiated ices but the HNCO/NH_2CHO ratio does not match observations. A tight empirical correlation between the abundances of HNCO and NH_2CHO has been observed using single dish observations (López-Sepulcre et al. 2015; Mendoza et al. 2004). This correlation between the abundances of these species is nearly linear and spans several orders of magnitude, suggesting that the two molecules are chemically related. ALMA observations by Coutens et al. (2016) of IRAS 16293-2422 show that the deuterium fractions in HNCO and NH_2CHO are very similar, also implying a chemical link.

On the other hand, the laboratory study by Noble et al. (2015) finds that hydrogenation of HNCO by deuterium bombardment does not lead to NH_2CHO in detectable quantities, while Barone et al. (2015) find that the H_2CO+NH_2 reaction can reproduce the abundance of NH_2CHO in IRAS16293-2422, a Sun-like protostar. Codella et al. (2017) observed a shock near L1157-B1 using interferometric observations. Through these observations and follow-up chemical modeling, they concluded that NH_2CHO is made efficiently in the gas phase from H_2CO, at least in this source. Recent work by Quénard et al. (2018) modeling the formation of HNCO and NH_2CHO and other peptide-bearing molecules shows a correlation between the abundances of H_2CO and NH_2CHO as well as between HNCO and NH_2CHO without using hydrogenation. The possibility exists that different types of sources (shocked regions, outflow cavities, accretion disks, protostellar envelopes, etc.) may have different dominant formation routes, but this possibility stands to be examined.

2. Observational tests

2.1. Moment maps

Using ALMA Cycle 2 observations of three high-mass star-forming regions (shown in Figure 2) with six sub-sources (listed in Table 1) containing young O-type stars, we studied moment maps (integrated intensity, velocity, and velocity dispersion) of 1-3 transitions each of HNCO, H_2CO, and NH_2CHO (all transitions studied are listed in Table 2) comparing the emission peak position, velocity gradient, and gas velocity dispersion. Comparisons were made under the assumption that similarities in gas peak, velocity gradient, and dispersion imply that the compared species are in the same gas and are therefore chemically related.

In these conference proceedings, we present the analysis of G345 as an example. The full report can be found in Allen et al.

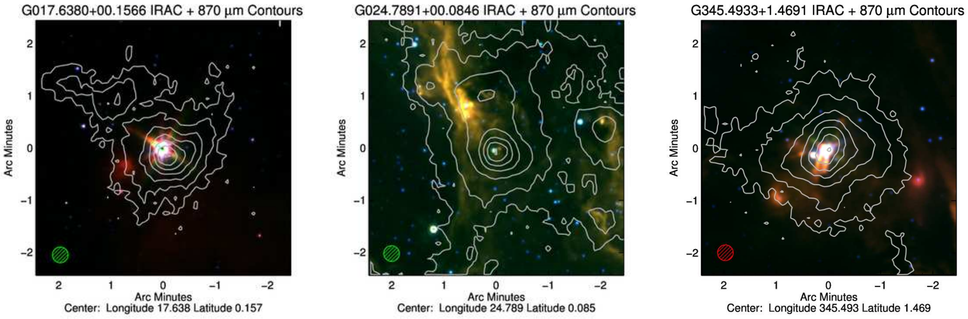

Fig. 2. Spitzer IRAC images overlaid with ATLASGAL contours of the star forming regions: (left) G17.64+0.16, (center) G24.78+0.08, and (right) G345.49+1.47 (from RMS database).

Table 1. Spectral extraction points for line identification and spectral modeling. These points coincide with the NH_2CHO peak used for each source. N_{core} is determined as in Sánchez-Monge et al. (2014) using the continuum intensity at the spectral extraction point assuming a T_{ex} of 100 K, a dust opacity of 1.75 cm^2 g^{-1}, and a gas-to-dust ratio of 100. Check mark (✓) symbols indicate the detection of H(30)α emission toward the sub-source.

Source	Right Ascension (J2000)	Declination (J2000)	N_{core} (cm^{-2})	H(30)α
G17	18:22:26.370	-13:30:12.06	2.8×10^{25}	✓
G24 A1	18:36:12.544	-07:12:11.14	9.1×10^{24}	✓
G24 A2(N)	18:36:12.465	-07:12:09.61	1.7×10^{24}	
G24 A2(S)	18:36:12.471	-07:12:10.09	1.4×10^{24}	
G345 main	16:59:41.628	-40:03:43.63	2.3×10^{26}	✓
G345 NW spur	16:59:41.586	-40:03:43.15	4.5×10^{25}	

Table 2. Transition properties from the CDMS (Endres et al. 2016). The last column shows the sources in which this transition appeared. HNCO (3) has a much higher upper energy level than the other transitions, so we consider it cautiously.

Species	Transition	Frequency (MHz)	E_{up} (K)	A_{ij} (s^{-1})	Sources
HNCO (1)	$10_{0,10}$-$9_{0,9}$	219798.27	58.0	1.47×10^{-4}	G24
HNCO (2)	$10_{1,9}$-$9_{1,8}$	220584.75	101.5	1.45×10^{-4}	G17, G345
HNCO (3)	$10_{3,7}$-$9_{3,6}$	219656.77	432.9	1.20×10^{-4}	G24, G345
NH_2CHO (1)	$10_{1,9}$-$9_{1,8}$	218459.21	60.8	7.47×10^{-4}	G17, G345
NH_2CHO (2)	$11_{2,10}$-$10_{2,9}$	232273.64	78.9	8.81×10^{-4}	G24
H_2CO (1)	$3_{0,3}$-$2_{0,2}$	218222.19	20.9	2.82×10^{-4}	G17, G24, G345
H_2CO (2)	$3_{2,2}$-$2_{2,1}$	218475.63	68.1	1.57×10^{-4}	G17, G24, G345
H_2CO (3)	$3_{2,1}$-$2_{2,0}$	218760.07	68.1	1.58×10^{-4}	G17, G24, G345

2019 (in review). G345 can be divided into two sub-sources: Main, which shows very strong continuum, weak H(α) emission, and little chemical complexity; and NW spur, which is very chemically complex but has very weak continuum emission. Figure 3 shows the contours H_2CO and HNCO vs. NH_2CHO. The difference between the emis-

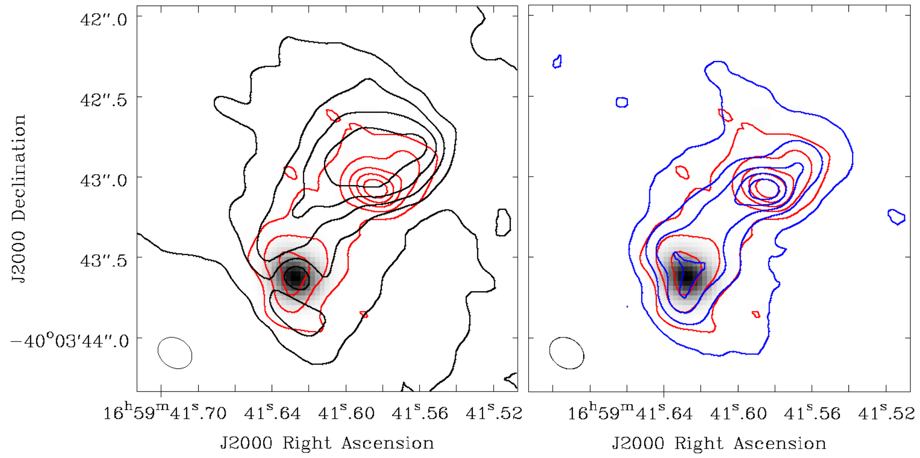

Fig. 3. G345 moment 0 maps (contours) overlaid on the dust continuum (greyscale). *Left:* the black contours show the H_2CO (3) transition (E_{up}=68.1 K) from 5σ (0.027 Jy/beam km s^{-1}) to a peak of 0.402 Jy/beam km s^{-1}. The red contours show NH_2CHO (1) emission (E_{up}=60.8 K) from 5σ (0.020 Jy/beam km s^{-1}) to 0.242 Jy/beam km s^{-1}. *Right:* the blue contours show the extent of the HNCO (2) emission (E_{up}=101.5 K) from 5σ (0.014 Jy/beam km s^{-1}) to 0.428 Jy/beam km s^{-1} with the red contours showing NH_2CHO (as in the left frame).

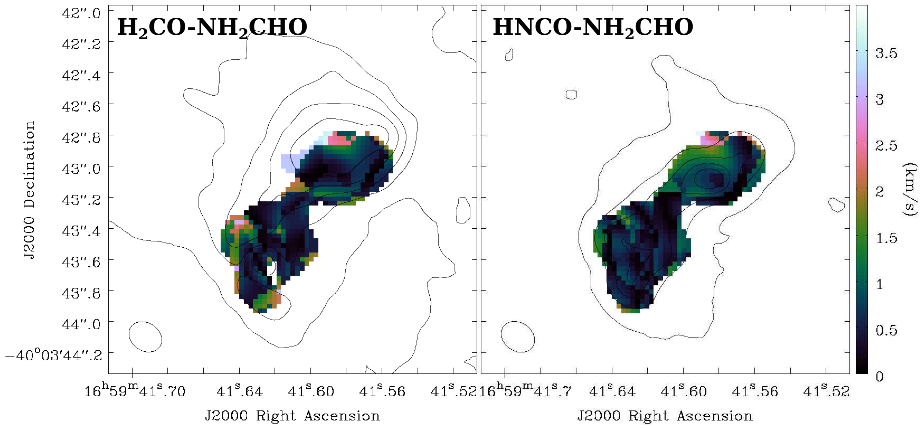

Fig. 4. Velocity difference (from moment 1 maps) at each pixel in G345 between (left) H_2CO (2) and NH_2CHO (1) and (right) HNCO (2) and NH_2CHO (1). The contours show the integrated intensity maps for H_2CO (2) and HNCO (2) as in Figure 3. The velocity scale is the same for both panels.

sion peaks for G345 Main were ~0.2″ for H_2CO and NH_2CHO and ~0.04 for the HNCO (2) and NH_2CHO. For G345 NW spur, these differences were 0.2″ and 0.03″, respectively. Figure 4 shows the difference in velocity values (v_{H2CO}-v_{NH2CHO} (left) and v_{HNCO}-v_{NH2CHO} (right)) for each pixel with darker colors indicating a small difference and lighter colors a greater difference. For G345, the moment maps of HNCO are more similar to NH_2CHO than those of H_2CO. We see from the summary of map analysis results in Table 3 that the peak positions and dispersion maps favor HNCO slightly over H_2CO in similarity with NH_2CHO and the velocity dispersion maps for HNCO are almost always most similar to NH_2CHO. From these overall results, it seems that HNCO has a slightly stronger relationship with NH_2CHO.

2.2. Spectral line modeling

In addition to analyzing the moment maps, we also used the XCLASS[1] spectral line modeling software (Möller et al. 2017) assuming local thermal equilibrium (LTE) to determine the excitation temperature (T_{ex}), column density (N_{col}), line width (FWHM), and velocity offset (v_{LSR}) for each of our focus species and compare them to each other. This software models the data by solving the radiative transfer equation for an isothermal object in one dimension, taking into account source size and dust opacity.

Comparing the model results obtained using spectra extracted from pixels coinciding with the NH_2CHO emission peaks, we found no significant relationship between T_{ex} values, or FWHM of the three species. There was a strong relationship (R^2=0.93 where 1 is perfectly correlated) between the abundances (X; the modeled N_{col} value divided by the N_{core} value calculated from the dust continuum) of HNCO and NH_2CHO. This relationship was previously investigated by López-Sepulcre et al. (2015) whose best power-law fit equation from that paper was reported to be $X(NH_2CHO) = 0.04\ X(HNCO)^{0.93}$. Figure 5 shows that the best fit in this work is $X(NH_2CHO)=0.03(\pm0.02)\ X(HNCO)^{0.92(\pm0.08)}$ and that correlations can be found between each pair of species abundances, but the strongest, by far, is that of HNCO and NH_2CHO. There is also a stronger correlation between the velocity shifts of HNCO and NH_2CHOthan H_2CO and NH_2CHO (R^2 of 0.95 vs. 0.48).

2.3. Caveats and future work

The opacity of the H_2CO transitions investigated here cannot be discounted. It is possible that the greater differences in spatial distribution, velocity, and dispersion between H_2CO and NH_2CHO compared to HNCO arise from optical depth issues. This is being investigated in a follow-up study involving isotopologues. It can also be seen in Table 3 that many of the moment map differences between each potential parent species and NH_2CHO are the equal within errors. This will be remedied in the future by using higher spatial and velocity resolution observations.

3. Conclusions

We present an observational study of two species that are potentially chemically related (HNCO and H_2CO) to NH_2CHO. In our spectral modeling, we confirm the single dish relationship between the abundances of HNCO and NH_2CHO demonstrated in López-Sepulcre et al. (2015) using interferometric observations. Our map analyses favor HNCO as chemically related to NH_2CHO. The abundance correlation between HNCO and NH_2CHO is stronger than the correlation between H_2CO and NH_2CHO but both are well correlated. It is possible that both formation processes are important in creating this species, or that different environments favor one process over the other. Dedicated studies using more transitions and isotopologues in a more diverse selection of sources (high- and low-mass protostars, young stellar objects with disks, outflow regions, etc.) will shed light on this relationship.

Acknowledgements. This work makes use of ALMA data: ADS/JAO.ALMA 2013.1.00489.S (P.I. Riccardo Cesaroni). ALMA is a partnership of ESO (representing its member states), NSF (USA) and NINS (Japan), together with NRC (Canada) and NSC and ASIAA (Taiwan), in cooperation with the Republic of Chile. The Joint ALMA Observatory is operated by ESO, AUI/NRAO and NAOJ. The PhD project of V. Allen was funded by NWO and SRON. V. Allen's research is supported by an appointment to the NASA Postdoctoral Program at the NASA Goddard Space Flight Center, administered by Universities Space Research Association under contract with NASA. V.M.R. is funded by the the European Union's Horizon 2020 research and innovation programme under the Marie Skłodowska-Curie grant agreement No 664931.

[1] Available from: `https://xclass.astro.uni-koeln.de/`

Table 3. Summary of results from map analyses. The check symbol (✓) indicates the species with the emission peak closest to the NH_2CHO peak, velocity-difference histogram center nearest to zero, or dispersion-difference histogram center nearest to zero. Equals signs (=) indicate that the parameters were equal for both HNCO and H_2CO within errors.

	HNCO			H_2CO		
Source	**Peak**	**Velocity**	**Dispersion**	**Peak**	**Velocity**	**Dispersion**
G17		=	✓	✓	=	
G24 A1	✓	✓	✓			
G24 A2(N)	✓		✓		✓	
G24 A2(S)	=	=	✓	=	=	
G345 Main	✓	=	✓		=	
G345 NW spur	✓	=	=		=	=

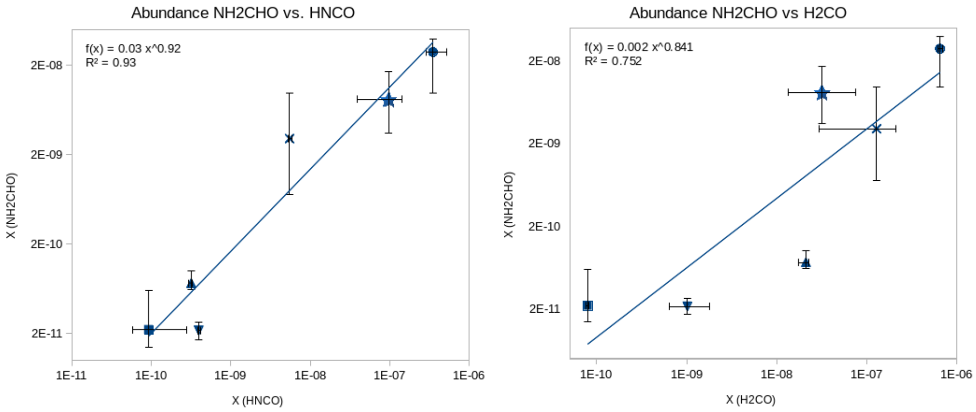

Fig. 5. XCLASS determined abundance comparison between $NH_2CHO$and HNCO (left), $NH_2CHO$and H_2CO (right). The symbols correspond to different regions as follows: G17 is an upward triangle, G24 A1 is an 'x', G24 A2(N) is a star, G24 A2(S) is a circle, G345 main is a square, and G345 NW spur is a downward triangle.

References

Barone, V., Latouche, C., Skouteris, D., et al. 2015, MNRAS, 453, L31

Charnley, S. B. 1997, in Astronomical and Biochemical Origins and the Search for Life in the Universe, eds. C. Batalli Cosmovici, et al. (Editrice Compositori, Bologna), IAU Colloquium, 161, 89

Codella, C., Ceccarelli, C., Caselli, P., et al. 2017, A&A, 605, L3

Coutens, A., Jørgensen, J. K., van der Wiel, M. H. D., et al. 2016, A&A, 590, L6

Endres, C. P., Schlemmer, S., Schilke, P., et al. 2016, J. Mol. Spectrosc., 327, 95

Kahane, C., Ceccarelli, C., Faure, A., & Caux, E. 2013, ApJ, 763, L38

Kaňuchová, Z., Boduch, P., Domaracka, A., et al. 2017, A&A, 604, 68

López-Sepulcre, A., Jaber, A. A., Mendoza, E., et al. 2015, MNRAS, 449, 2438

Mendoza, E., Lefloch, B., López-Sepulcre, A., et al. 2014, MNRAS, 445, 151

Möller, T., Endres, C. & Schilke, P. 2017, A&A, 598, A7

Noble, J. A., Theule, P., Congiu, E., et al. 2015, A&A, 576, A91

Quénard, D., Jiménez-Serra, I., Viti, S., et al. 2018, MNRAS, 474, 2796

Saladino, R., Crestini, C., Pino, S., et al. 2012, Physics of Life Reviews, 9, 84

Sánchez-Monge, Á., Beltrán, M. T., Cesaroni, R., et al. 2014, A&A, 569, A11